Journal of Zhejiang University-SCIENCE A (Applied Physics & Engineering)
ISSN 1673-565X (Print); ISSN 1862-1775 (Online)
www.jzus.zju.edu.cn; www.springerlink.com
E-mail: jzus@zju.edu.cn

A structural morphogenesis method based on a linkage mechanism system*

Gui-gang TU[1], Chang-yu CUI[†‡1,2], Guang-chun ZHOU[1,2]

[1]*School of Civil Engineering, Harbin Institute of Technology, Harbin 150090, China*

[2]*Key Lab of Smart Prevention and Mitigation of Civil Engineering Disasters of the Ministry of Industry and Information Technology, Harbin 150090, China*

[†]E-mail: cuichangyu1963@hit.edu.cn

Received Oct. 7, 2017; Revision accepted Mar. 9, 2018; Crosschecked Sept. 12, 2018

Abstract: This paper presents an elements-grouped morphogenesis method for the design of grid shells based on finding the linkage mechanism system shape that corresponds to the state of minimum potential energy. This method assigns the elements to several groups according to architectural design intentions and requirements to optimize a structural shape. A shape transformation equation is derived to constrain the total length of elements in each element group in the morphogenesis process and the generalized inverse matrix theory is then used to resolve the equation. The positions of nodes are, thus, progressively updated until the system reaches the minimum potential energy state. This method is characterized by the settings of element groups, temporary elements, and temporary forces. Finally, several numerical examples illustrate the characteristics and effectiveness of the proposed method.

Key words: Morphogenesis; Elements-grouped; Linkage mechanism; Length constraint; Self-adjustment of length
https://doi.org/10.1631/jzus.A1700545 **CLC number:** TU318

1 Introduction

Engineers have always used a variety of ways to meet all kinds of design intentions and architectural requirements. Previously, physical experiments such as soap films and hanging models were used to generate architectural shapes of high mechanical performance (Isler, 1994; Adriaenssens et al., 2014). Soap films are applied to generate pre-stressed structures whose shapes are similar to minimal surfaces and hanging models are used to determine the shapes of structures in pure compression. These physical experimental methods use the characteristic of the physical model that it cannot accept bending moments and thus demonstrate the rational shapes for structures under applied load.

In recent years, numerical methods have been gradually replacing physical model experiments as they allow for diversification, convenience, economy, etc. Structural morphogenesis is based on these numerical methods, including structural optimization methods and form finding methods, aiming at generating structures which can combine architectural appearance and mechanical performance. Structural optimization methods such as evolutionary structural optimization (Xie and Steven, 1993) and sensitivity analysis (Cui et al., 2014) can be applied to various kinds of structures while form finding mainly specializes in generating structures in pure compression or tension (Bletzinger et al., 2005). The stiffness matrix method (Siev and Eidelman, 1964; Haug and

‡ Corresponding author
* Project supported by the National Natural Science Foundation of China (No. 51578185)
ORCID: Gui-gang TU, https://orcid.org/0000-0002-6154-9457; Chang-yu CUI, https://orcid.org/0000-0001-9163-8648

Powell, 1972; Argyris et al., 1974), the force density method (Schek, 1974), and the dynamic relaxation (DR) method (Day, 1965; Barnes, 1977) were earlier form finding methods that were typically applied to cable-net structures. Form finding methods were then extended to membrane structures (Haber and Abel, 1982; Barnes, 1988; Maurin and Motro, 1998; Bletzinger and Ramm, 1999). In addition, scholars and engineers explored many new methods of form finding. Hangai and Kawaguchi (1987) presented a method that used generalized inverse matrix theory to determine the rational structural shape. Gosling and Lewis (1996) presented an algorithm for generating minimal surfaces based on a finite element method and DR. Adriaenssens and Barnes (2001) and Barnes et al. (2013) proposed and studied thoroughly the spline elements in the DR method. Maurin and Motro (2004) presented a form finding method for concrete shells focusing on the numerical calculation of geometry and stress distribution. Kilian and Ochsendorf (2005) used particle-spring systems for determining structures in pure compression. Sánchez et al. (2007) proposed a method that combines a form finding technique with a surface-fitting approach. Block and Ochsendorf (2007) presented thrust network analysis for compression-only vaulted surfaces and networks. Pauletti and Pimenta (2008) developed a natural force density method which is an extension of the force density method. Bagrianski and Halpern (2014) presented a prescriptive DR method that can achieve element length prescription. Alic and Persson (2016) combined the DR method and non-uniform rational B-Splines. The methods mentioned above are used for tension structures (cable-net and membrane structures) and shell structures. Also some scholars attempted to develop form finding methods to determine the rational shapes of bridge structures (Descamps et al., 2011; Jorquera Lucerga and Armisen, 2012; Bel Hadj Ali et al., 2010) and tensegrity structures (Moored and Bart-Smith, 2009; Bel Hadj Ali et al., 2011; Zhang et al., 2015). Especially in the form finding of tensegrity structures, the cable elements linked to each other sometimes need to be treated as one cable in order to simulate a continuous cable, which can be seen as an approach of element grouping. So far, the element grouping approach has not been applied to the morphogenesis of grid shells, but its grouping manner can be extended in order to generate more shapes for architectural design. We therefore attempt to adopt a generalized grouping approach and an innovative strategy to control the total length of each group of elements to enrich the choices for structural morphogenesis.

In this paper, the elements-grouped method is proposed for generating rational structural shapes. This method groups the elements in the linkage mechanism system and searches the shape of the system corresponding to the minimum potential energy, under the prescriptive total length of the elements in each element group. The structure with the same shape of the mechanism system corresponding to the minimum potential energy carries the given load in compression with minimal bending moments. The element group setting determines the mode of the length constraint, which characterizes the elements-grouped method. Correspondingly, this paper first derives the shape transformation equation and then describes its numerical implementation. Functions and characteristics of the proposed method are then illustrated by several design examples. Finally, two large-scale design problems are solved to validate the effectiveness of this method in structural morphogenesis.

2 Elements-grouped method based on the linkage mechanism system

2.1 Rational and constraints included in the optimization problem

The potential energy of a linkage mechanism system is associated with nodal forces and nodal positions in space. When the system is in the minimum potential energy state there are only axial forces in it. This principle can be used in structural morphogenesis. Fig. 1a shows a structure under load $\boldsymbol{F}$ and the bending moment in the structure is not zero. The rigid joint is first turned into a hinged joint so that the structure becomes a mechanism (Fig. 1b). Then, the mechanism shape changes until the potential energy with respect to load $\boldsymbol{F}$ becomes minimal (Fig. 1c). In these two steps, the potential energy increment is calculated as $-\boldsymbol{F}\cdot\boldsymbol{S}$ (where $\boldsymbol{S}$ is the nodal displacement vector). Finally, the hinged joint is turned into a rigid joint again and there is only axial force in the structure. This process generates a rational structural shape through searching for the mechanism shape

corresponding to the minimum potential energy. The optimized structure bears the load with only an axial force (Fig. 1d).

The elements in a linkage mechanism system are assigned to several element groups and the total length of the elements in each element group is constrained in the potential energy reduction process. Such a measure can bring some special functions in generating a structural shape. Fig. 2a shows a simple example of a linkage mechanism whose elements are grouped. In this linkage mechanism, there are five elements and three element groups. If an element group has more than one element, each element length is changeable while the total element length in this element group is constant and is referred to as the element group length. Fig. 2b shows the final shape of the linkage mechanism corresponding to the minimum potential energy under load $\boldsymbol{F}$. In this process, the element group lengths have the relations: $l_{11}=l'_{11}$, $l_{21}+l_{22}=l'_{21}+l'_{22}$, $l_{31}+l_{32}=l'_{31}+l'_{32}$. Different element group settings derive different functions. The length of the element in the first element group is constant and it can be seen as a rigid bar. The node linking the two elements in the second element group is a sliding node. The length of the left element transforms to the right element in the third group to make the potential energy of the mechanism decrease. In this process, the two elements can be imagined as a Bowden cable.

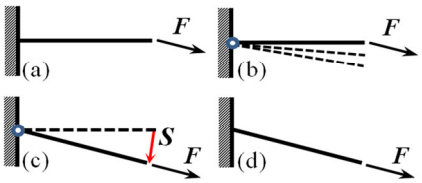

Fig. 1 Process of generating a rational structure
(a) Initial structure; (b) Initial linkage mechanism; (c) Generated linkage mechanism; (d) Generated structure

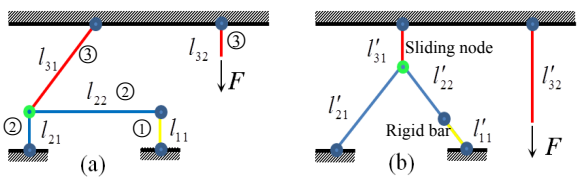

Fig. 2 Grouping of elements in a linkage mechanism system: (a) initial mechanism; (b) resultant mechanism

2.2 Mathematical model and shape transformation equation

The elements-grouped method finds the rational structural shape through searching for the linkage mechanism system shape corresponding to the minimum potential energy and the mathematical model can be expressed as

$$\begin{aligned} &E_{\mathrm{p}}(\boldsymbol{P})\to \text{minimum},\\ &\text{s.t.}\quad \boldsymbol{\Omega}\subseteq\boldsymbol{\Omega}_0,\\ &\qquad \boldsymbol{L}=\boldsymbol{L}_0, \end{aligned} \tag{1}$$

where $\boldsymbol{P}$ is the nodal coordinate vector of the linkage mechanism system in one state and $E_{\mathrm{p}}(\boldsymbol{P})$ is the potential energy of the linkage mechanism in this state; $\boldsymbol{\Omega}$ is the structural shape and $\boldsymbol{\Omega}_0$ is the design space; $\boldsymbol{L}$ is the element group length vector and $\boldsymbol{L}_0$ is the initial element group length vector. The initial model and the element group can be set according to the design intent of architect. Then, the corresponding shape transformation equation is derived under the condition that the element group length keeps constant. Finally, the solution that makes the nodal displacements occur along the direction of the steepest descent of potential energy is obtained by using a generalized inverse matrix and used to update the nodal positions. The relative calculations in this process are as follows:

Firstly, a shape transformation equation is derived to constrain the element group length in the shape transformation process. The ith element group length is expressed as

$$l_i=\sum_{j=1}^{n_i}\sqrt{(\boldsymbol{P}_{ij_2}-\boldsymbol{P}_{ij_1})^{\mathrm{T}}(\boldsymbol{P}_{ij_2}-\boldsymbol{P}_{ij_1})}, \tag{2}$$

where $\boldsymbol{P}_{ij_1}$ and $\boldsymbol{P}_{ij_2}$ are the nodal coordinate vectors of the jth element in the ith element group, and n_i is the number of elements in the ith element group.

$$\boldsymbol{P}_{ij_k}=(x_{ij_k}\quad y_{ij_k}\quad z_{ij_k})^{\mathrm{T}},\quad k=1,\ 2. \tag{3}$$

A common controlling variable t is defined to govern the variation of coordinates. The derivative of the element group length with respect to t is

$$\begin{aligned}\frac{\partial l_i}{\partial t}=\dot{l}_i&=\sum_{j=1}^{n_i}\left(\frac{(\boldsymbol{P}_{ij_2}-\boldsymbol{P}_{ij_1})^{\mathrm{T}}}{l_{ij}}\cdot\left(\frac{\partial \boldsymbol{P}_{ij_2}}{\partial t}-\frac{\partial \boldsymbol{P}_{ij_1}}{\partial t}\right)\right)\\&=\sum_{j=1}^{n_i}\left(\boldsymbol{\lambda}_{ij}^{\mathrm{T}}\cdot(\dot{\boldsymbol{P}}_{ij_2}-\dot{\boldsymbol{P}}_{ij_1})\right),\end{aligned}\tag{4}$$

where $\boldsymbol{\lambda}_{ij}$ and l_{ij} are the direction cosine vector and length of the jth element in the ith element group, respectively. Eq. (4) can be rewritten as

$$\dot{l}_i=\begin{bmatrix}\boldsymbol{a}_{i1} & \boldsymbol{a}_{i2} & \cdots & \boldsymbol{a}_{in}\end{bmatrix}\begin{bmatrix}\dot{\boldsymbol{P}}_{i1}\\ \dot{\boldsymbol{P}}_{i2}\\ \vdots\\ \dot{\boldsymbol{P}}_{in}\end{bmatrix},\tag{5}$$

where n is the number of nodes in the ith element group. Eq. (5) expresses the relationship of the change rate of the ith element group length with nodal velocities. Assuming that the linkage mechanism system has m element groups, the element group length vector of the system is

$$\boldsymbol{L}=(l_1 \quad l_2 \quad \cdots \quad l_m)^{\mathrm{T}}.\tag{6}$$

Take the derivative of $\boldsymbol{L}$ with respect to t

$$\dot{\boldsymbol{L}}=(\dot{l}_1 \quad \dot{l}_2 \quad \cdots \quad \dot{l}_m)^{\mathrm{T}}.\tag{7}$$

Eq. (5) expresses just one element group in the linkage mechanism system. Write Eq. (5) for all element groups in the mechanism system and then assemble them into a matrix equation after deleting the fixed nodes.

$$\dot{\boldsymbol{L}}=\boldsymbol{A}_{m\times\beta}\dot{\boldsymbol{P}},\tag{8}$$

where $\dot{\boldsymbol{P}}$ is the free nodal velocity vector of the linkage mechanism system, β is the number of degrees of freedom of the linkage mechanism system, and $\boldsymbol{A}$ is the coefficient matrix of the equation. Because the element group lengths are constrained, Eq. (8) can be rewritten as

$$\boldsymbol{A}_{m\times\beta}\dot{\boldsymbol{P}}=\boldsymbol{0}.\tag{9}$$

Thus, a shape transformation equation is obtained. Then, the inverse matrix theory is introduced to solve Eq. (9). Because $m<\beta$ in Eq. (9), the generalized inversed matrix theory is introduced to solve Eq. (9):

$$\dot{\boldsymbol{P}}=(\boldsymbol{I}_\beta-\boldsymbol{A}^{-}\boldsymbol{A})\cdot\boldsymbol{\alpha},\tag{10}$$

where $\boldsymbol{\alpha}$ is an arbitrary combination coefficient vector and $\boldsymbol{A}^{-}$ is the generalized inverse matrix of $\boldsymbol{A}$. $\boldsymbol{I}_\beta$ is the unit matrix. If the rank of $\boldsymbol{A}$ is r, then

$$q=\mathrm{rank}\left(\boldsymbol{I}_\beta-\boldsymbol{A}^{-}\boldsymbol{A}\right)=\beta-r.\tag{11}$$

Eq. (10) can be expressed as

$$\begin{aligned}\dot{\boldsymbol{P}}&=\begin{bmatrix}\boldsymbol{h}_1 & \boldsymbol{h}_2 & \cdots & \boldsymbol{h}_q\end{bmatrix}\boldsymbol{\alpha}\\&=\alpha_1\boldsymbol{h}_1+\alpha_2\boldsymbol{h}_2+\cdots+\alpha_q\boldsymbol{h}_q,\end{aligned}\tag{12}$$

where $\boldsymbol{h}_1$, $\boldsymbol{h}_2$, ⋯, $\boldsymbol{h}_q$ are the basis vectors of $(\boldsymbol{I}_\beta-\boldsymbol{A}^{-}\boldsymbol{A})$ which are the displacement modes of the linkage mechanism system. It should be noted that the solution obtained by Eq. (12) is non-unique.

2.3 Progressive morphogenesis process

In the progressive morphogenesis process of the elements-grouped method, the potential energy of the system is a function of the nodal coordinates under the given load. Reduction of potential energy derives from the optimization process of updating nodal coordinates, that is

$$E_{\mathrm{p}}(\boldsymbol{P}^0)>E_{\mathrm{p}}(\boldsymbol{P}^1)\cdots>E_{\mathrm{p}}(\boldsymbol{P}^i)\cdots>E_{\mathrm{p}}(\boldsymbol{P}^s),\tag{13}$$

where $\boldsymbol{P}^i$ and $E_{\mathrm{p}}(\boldsymbol{P}^i)$ are the nodal coordinate vector and the potential energy of the mechanism system, respectively, in the state i. Thus, an iteration process is formed to update the coordinates. When a linkage mechanism system transforms from state i to state i+1, the updated coordinate vector can be calculated by

$$\boldsymbol{P}^{i+1}=\boldsymbol{P}^i+\Delta\boldsymbol{P}^i=\boldsymbol{P}^i+\dot{\boldsymbol{P}}^i\Delta t.\tag{14}$$

In state i+1, the potential energy is

$$E_{\mathrm{p}}(\boldsymbol{P}^{i+1})=E_{\mathrm{p}}(\boldsymbol{P}^i)+\Delta E_{\mathrm{p}}(\boldsymbol{P}^i),\tag{15}$$

where $\Delta E_{\mathrm{p}}(\boldsymbol{P}^i)$ is the potential energy increment from state i to state i+1. The potential energy increment is calculated by

$$\Delta E_{\mathrm{p}}(\boldsymbol{P}^i)=-((\dot{\boldsymbol{P}}^i)^{\mathrm{T}}\Delta t)\cdot\boldsymbol{F}=-(\dot{\boldsymbol{P}}^i)^{\mathrm{T}}\cdot\boldsymbol{F}\Delta t, \quad (16)$$

where $\boldsymbol{F}$ is the nodal force vector. Substituting Eq. (12) into Eq. (16), $\Delta E_{\mathrm{p}}(\boldsymbol{P}^i)$ can be written as

$$\Delta E_{\mathrm{p}}(\boldsymbol{P}^i)=-(\alpha_1\boldsymbol{h}_1+\alpha_2\boldsymbol{h}_2+\cdots+\alpha_q\boldsymbol{h}_q)^{\mathrm{T}}\cdot\boldsymbol{F}\Delta t. \quad (17)$$

Since $\dot{\boldsymbol{P}}^i$ calculated by Eq. (12) is non-unique, $\Delta E_{\mathrm{p}}(\boldsymbol{P}^i)$ is also non-unique. In order to find the minimum potential energy state quickly, the gradient method is used to find the solution of Eq. (9) that yields the largest reduction of potential energy under the given Δt. The combination coefficient vector $\boldsymbol{\alpha}$ in Eq. (12) can be calculated by

$$\boldsymbol{\alpha}=-\begin{bmatrix}\dfrac{\partial\Delta E_{\mathrm{p}}}{\partial\alpha_1}\\ \dfrac{\partial\Delta E_{\mathrm{p}}}{\partial\alpha_2}\\ \vdots\\ \dfrac{\partial\Delta E_{\mathrm{p}}}{\partial\alpha_q}\end{bmatrix}=\begin{bmatrix}\boldsymbol{h}_1^{\mathrm{T}}\boldsymbol{F}\\ \boldsymbol{h}_2^{\mathrm{T}}\boldsymbol{F}\\ \vdots\\ \boldsymbol{h}_q^{\mathrm{T}}\boldsymbol{F}\end{bmatrix}. \quad (18)$$

Thus, Eq. (12) can be written as

$$\dot{\boldsymbol{P}}^i=\left(\boldsymbol{h}_1^{\mathrm{T}}\boldsymbol{F},\boldsymbol{h}_2^{\mathrm{T}}\boldsymbol{F},\cdots,\boldsymbol{h}_q^{\mathrm{T}}\boldsymbol{F}\right)\begin{bmatrix}\boldsymbol{h}_1\\ \boldsymbol{h}_2\\ \vdots\\ \boldsymbol{h}_q\end{bmatrix}. \quad (19)$$

The increment of nodal coordinates $\Delta\boldsymbol{P}^i$ is

$$\Delta\boldsymbol{P}^i=\dot{\boldsymbol{P}}^i\Delta t=\left(\boldsymbol{h}_1^{\mathrm{T}}\boldsymbol{F},\boldsymbol{h}_2^{\mathrm{T}}\boldsymbol{F},\cdots,\boldsymbol{h}_q^{\mathrm{T}}\boldsymbol{F}\right)\begin{bmatrix}\boldsymbol{h}_1\\ \boldsymbol{h}_2\\ \vdots\\ \boldsymbol{h}_q\end{bmatrix}\Delta t. \quad (20)$$

Thus, the updated nodal coordinate vector is obtained:

$$\boldsymbol{P}^{i+1}=\boldsymbol{P}^i+\left(\boldsymbol{h}_1^{\mathrm{T}}\boldsymbol{F},\boldsymbol{h}_2^{\mathrm{T}}\boldsymbol{F},\cdots,\boldsymbol{h}_q^{\mathrm{T}}\boldsymbol{F}\right)\begin{bmatrix}\boldsymbol{h}_1\\ \boldsymbol{h}_2\\ \vdots\\ \boldsymbol{h}_q\end{bmatrix}\Delta t. \quad (21)$$

Substituting Eq. (18) into Eq. (17), the potential energy increment can be calculated as

$$\Delta E_{\mathrm{p}}(\boldsymbol{P}^i)=-[(\boldsymbol{h}_1^{\mathrm{T}}\boldsymbol{F})^2+(\boldsymbol{h}_2^{\mathrm{T}}\boldsymbol{F})^2+\cdots+(\boldsymbol{h}_q^{\mathrm{T}}\boldsymbol{F})^2]\Delta t. \quad (22)$$

When $\Delta E_{\mathrm{p}}(\boldsymbol{P}^i)$ approaches to zero, it means that the linkage mechanism system has reached a steady state and the potential energy cannot change. Therefore, the criterion for judging convergence is proposed as

$$\frac{\Delta E_{\mathrm{p}}(\boldsymbol{P}^i)}{\Delta E_{\mathrm{p}}(\boldsymbol{P}^0)}\le\varepsilon \ \text{ or } \ \Delta E_{\mathrm{p}}(\boldsymbol{P}^i)\le\varepsilon, \quad (23)$$

where ε is the threshold value. So far, in the architectural scheme design stage, the morphogenesis method can be summarized as follows:

1. Determine the initial shape according to the design space, architectural intention, structural and visual conditions.

2. Set the element groups and apply the load in consideration of the objective structure characteristics and practical working conditions.

3. Derive the shape transformation equation and calculate the nodal velocity vector by Eq. (19).

4. Update the nodal coordinates by Eq. (21) and calculate the potential energy increment by Eq. (22).

5. Repeat steps 2 to 4 until the convergence condition (Eq. (23)) is achieved.

6. Evaluate the resulting structural shape and check whether it meets the architectural and structural requirements. If all the requirements are met, the further design can be carried out. Otherwise, adjust the related influencing factors, and then return to step 2.

The value of step size Δt is determined through trial computation considering the numerical error (change of element group length) and convergence. A smaller Δt is recommended to ensure accuracy of the resultant shape. In the proposed method, there is no nodal equilibrium equation (dynamic equilibrium).

The progressive morphogenesis of the proposed method implies that the applied load does work on the mechanism system under the element group length constraint. When the load no longer works on the mechanism system, the system reaches a steady state. The topology of member-connection, boundary condition, load, element groups, and element lengths are the factors that influence the final shape.

3 Characteristics and applicability of the proposed method

In this section, several examples are given to illustrate the characteristics and applicability of the elements-grouped method developed in this research. Basically, the specific characteristics of the elements-grouped method are derived from the element group settings, and the effects of the element group setting on the resultant shape of system are shown in the examples. When the morphogenesis is completed, the mechanism system is translated into the structure by translating the hinged joints into rigid joints. A finite element analysis is used to evaluate the mechanical properties of the generated structure, in which the elastic modulus is 200 GPa, Poisson's ratio is 0.3, and all the members in the structure are treated as beam elements.

Fig. 3 shows the initial model of the linkage mechanism. The nodes at four corners are fixed and the vertical upward force acting on each node is 1.0 kN.

For investigating the effects of different element group settings on the resultant shape, three setting schemes as shown in Figs. 4a–4c are implemented. In Figs. 4a–4c, the bold line represents an element group. More specifically, (I) each element is set as one element group; (II) the elements in line are set as one element group; (III) the elements that are parallel to each other in a row or column are set as one element group. It is important to note that each element in the four edges is set as one element group in the three schemes. Figs. 4d–4f are the resultant shapes from the same initial shape (Fig. 3) but with different element group settings (Figs. 4a–4c), respectively. Differences between the three resultant shapes are

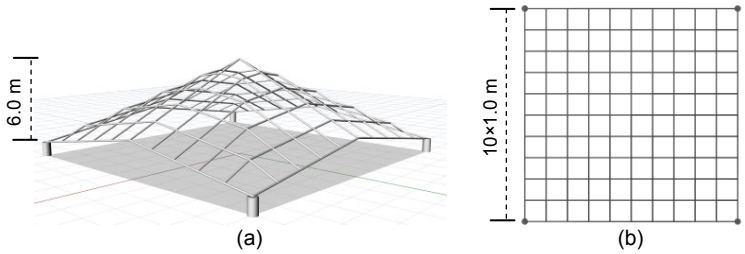

Fig. 3 Initial configuration of a linkage mechanism: (a) side view; (b) top view

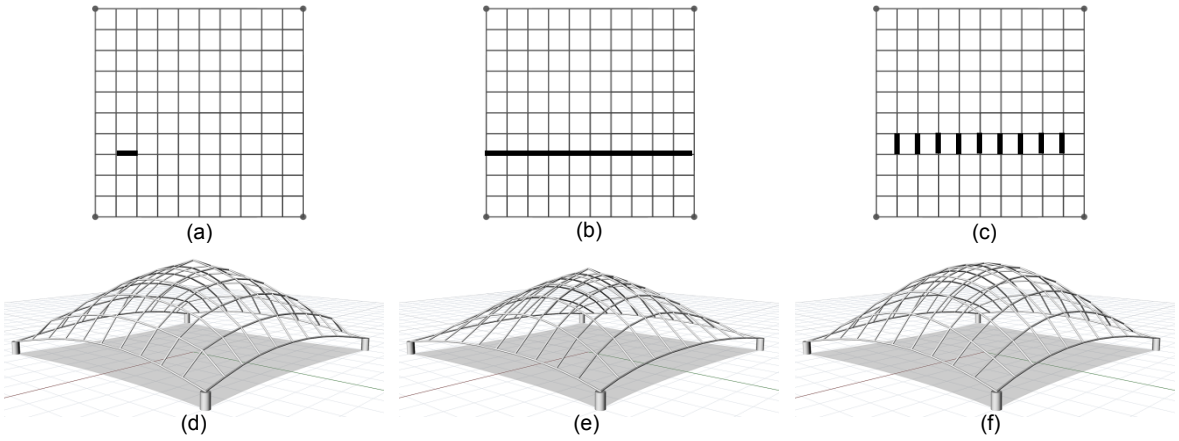

Fig. 4 Settings of element group and the resultant shapes

(a) Scheme (I); (b) Scheme (II); (c) Scheme (III); (d) Resultant shape for scheme (I); (e) Resultant shape for scheme (II); (f) Resultant shape for scheme (III)

obvious. For the shape in Fig. 4d, each element length is the same as that of the initial model because each element is set as one element group and its length is constrained. From Fig. 4e, the element lengths have changed and the shape is sharper compared with that in Fig. 4d. The element lengths in Fig. 4f have also changed and the shape becomes smooth and full, particularly, the spire of the initial structure disappears. The shapes in Figs. 4e and 4f break the limitation of the initial shape to some extent compared with the resultant shape in Fig. 4d. In the three schemes, the step size Δt is 0.001.

In scheme (I), the example simulates a rigid-bar hanging model experiment because the length of each bar in the mechanism is constrained. In scheme (II), the example simulates a hanging model with sliding nodes because we constrain the total length of the elements in line. In scheme (III), the elements in the same element group can be seen as a Bowden cable. These characteristics are derived from the length constraint modes (element group setting).

The shape transformation equation constrains the sum of the element lengths in each element group, and the lengths of elements in the same element group can transfer from one element to another if there is more than one element. Compared with the element group setting scheme (I), the schemes (II) and (III) make the linkage mechanism system more flexible. The function that the lengths of elements can transfer to each other in the same element group is called the length self-adjustment function of the elements-grouped method. Fig. 5 shows the potential energy increment changes of the mechanism system for the three schemes. The convergence speed for scheme (I) is the fastest because each element length is constrained and the shape change is smaller than those in the other two schemes.

In the finite element analysis, the chosen element type is a steel pipe with outer diameter of 8 cm and wall thickness of 1 cm. A vertical downwards nodal force (1.0 kN) acts on each node. Fig. 6 shows the moment and force distributions of the initial structure. The average bending moment is 2.04 kN·m and the maximum bending moment is 12.08 kN·m. The average axial force is 10.98 kN and the maximum axial force is 54.60 kN in the initial structure. Fig. 7 shows the moment and force distributions of the generated structures. For the three schemes, the average bending moments are 0.14 kN·m, 0.15 kN·m, and 0.11 kN·m while the average axial forces are 15.65 kN, 20.40 kN, and 15.70 kN, respectively. The maximum bending moments are 1.39 kN·m, 2.27 kN·m, and 1.58 kN·m, respectively. Through the optimization, the average bending moments decrease by 93.14%, 92.64%, and 94.61%, and the maximum bending moments decrease by 88.49%, 81.21%, and 86.92%. The generated structures carry the given load in compression with smaller bending moment.

DR is the usual method used in the form finding of a grid shell. The DR method needs to set a fictitious mass (referred to here as particle mass) at each node and to define the relationship between nodes in terms

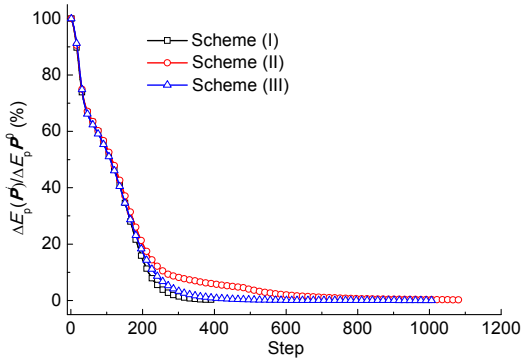

Fig. 5 Variation of potential energy increment in the design process

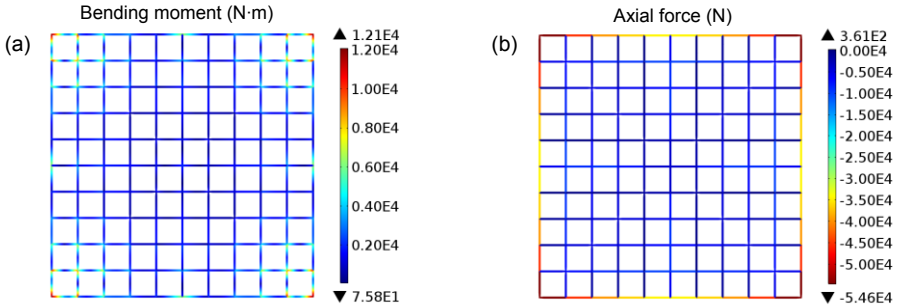

Fig. 6 Bending moment distribution (a) and force distribution (b) for the initial structure

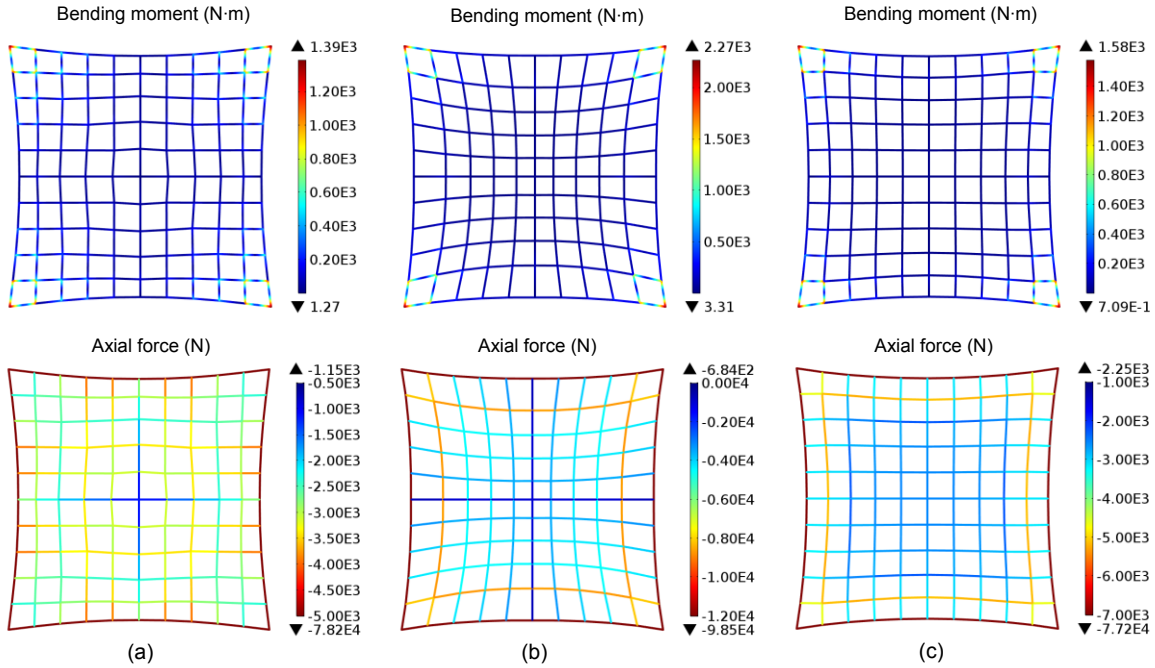

Fig. 7 Bending moment and force distributions for optimized structures
(a) Scheme (I); (b) Scheme (II); (c) Scheme (III)

of stiffness. In order to compare the method with the DR method, we apply the DR method to the initial model in Fig. 3 and the resultant shape is shown in Fig. 8a. Because the modified dynamic relaxation (MDR) method (Bel Hadj Ali et al., 2011) for the form finding of clustered tensegrity structures can simulate a continuous cable by treating the elements connected end to end as one cable, the MDR is applied to the initial model in Fig. 3 and the continuous cables are set referring to the scheme (II) in Fig. 4b. The resultant shape generated by the MDR method is shown in Fig. 8b. For the DR method and MDR method, each particle mass is 75 kg, axial stiffness is 1500 kN, and step size is 0.001. The particle mass has influence on convergence (Shan and Lan, 1994; Barnes, 1999). In this study, the particle mass is determined by trial calculation. Fig. 9 shows the moment and force distributions of the structures generated by the DR and MDR methods. In the structures generated by these methods, the average bending moments are 0.11 kN·m and 0.10 kN·m while the average axial forces are 10.40 kN and 11.04 kN; the maximum bending moments are 1.36 kN·m and 1.55 kN·m. The average bending moments decrease by 94.61% and 95.10%; the maximum bending moments decrease by 88.74% and 87.17%, respectively.

Similar to the DR and MDR methods, the proposed method can reduce the bending moments of the structures. It can be seen that the change trends of the shapes in Fig. 8a and Fig. 4d are similar, compared to the initial shape in Fig. 3a. Comparing the two shapes in Fig. 4e and Fig. 8b, the shapes generated by the two methods are similar. The heights of the shapes generated by the elements-grouped method are lower because the element group lengths are constrained. The DR method and MDR method can take account of material properties and the elements-grouped method is characterized by element grouping and element group length constraint.

In fact, the stable state with the minimum potential energy also corresponds to an equilibrium state. This can be demonstrated by the next example for generating a branching structure. The initial models are shown in Figs. 10a and 10c (p.852). Two element setting schemes are implemented. There are four element groups in Fig. 10a and three element groups in Fig. 10c. A temporary element is set to control the axial forces in the mechanism system. The temporary element is acted on by a temporary force to control the axial forces of the other elements in the group ①. The shapes in Figs. 10b and 10d are the resultant shapes corresponding to Figs. 10a and 10c, respectively.

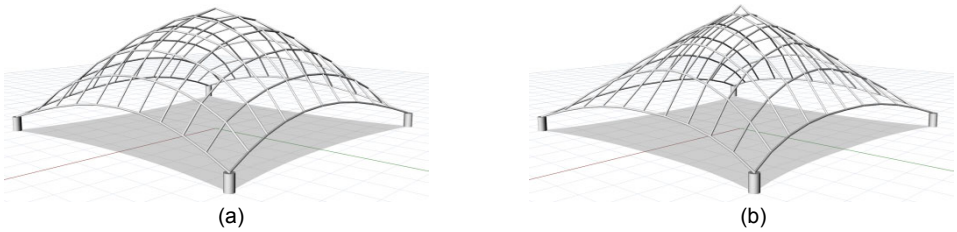

Fig. 8 Shapes generated by the DR method (a) and the MDR method (b)

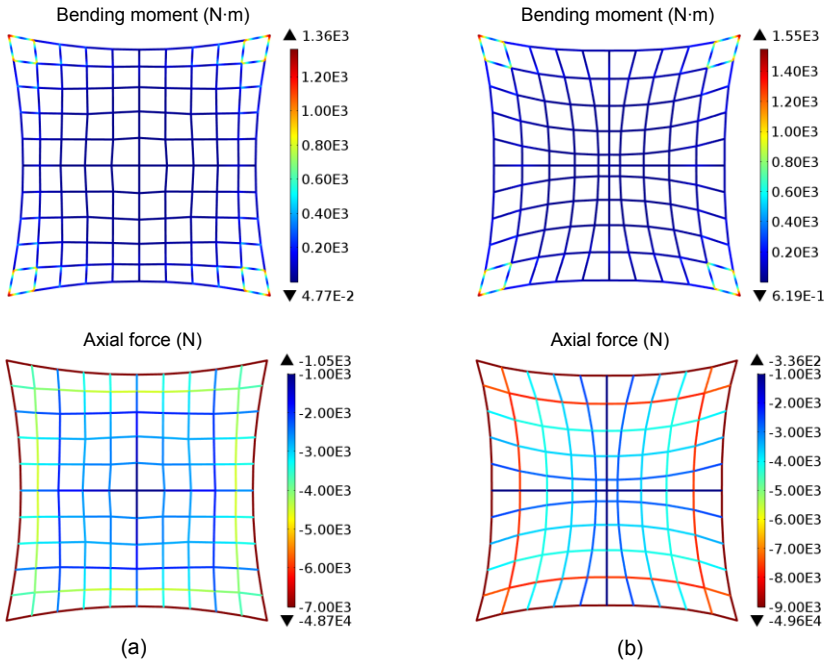

Fig. 9 Bending moment and force distributions for optimized structures: (a) DR; (b) MDR

According to the graphic statics, the internal axial forces are analyzed and shown in Figs. 10b and 10d. The axial forces of the elements controlled by the temporary element are very close to the temporary force. The self-adjustment of element lengths in each element group can also make the proposed method applicable for generating branching structures. It is of note that the temporary element plays two roles: a tensional force transmission medium and a station for transferring element lengths. The nodal coordinates of the shape in Fig. 10b are shown in Table 1.

For the next example, the initial model is shown in Fig. 11 to illustrate the application of the elements-grouped method in the case of tension structures. The nodes in the four edges are fixed. The elements connected head to tail are set as one element group so that there are 18 element groups in total, as marked in bold for one of them. In Fig. 11a, there are

Table 1 Nodal coordinates for the optimized configuration of Fig. 10b

Nodal number	x	y
1	−3.000000	0.000000
2	−1.000000	0.000000
3	1.000000	0.000000
4	3.000000	0.000000
5	−0.671618	−1.609690
6	1.034720	−0.730840
7	−0.108700	−2.461900
8	−0.108698	−4.460030
9	−6.000000	−1.000000
10	−6.000000	−12.760700

two vertical elements hanging on the edges in each element group (the bold one) and the nodal loads act on the two lowest nodes. This example simulates a tensioning experiment for the form finding of a hyperbolic paraboloid cable-net structure. In addition, these hanging elements are removed when transforming a mechanism system to a structure. The MDR method is also used on the same model. Figs. 12a and 12b show that the two methods obtain the same shape. The temporary elements are useless

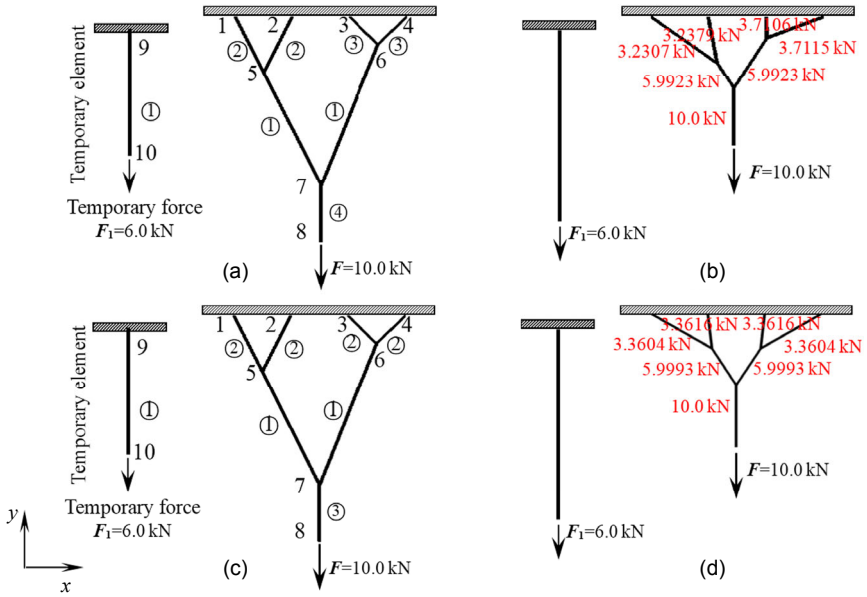

Fig. 10 Morphogenesis of branching structures

(a) The first initial model; (b) The first generated structure; (c) The second initial model; (d) The second generated structure

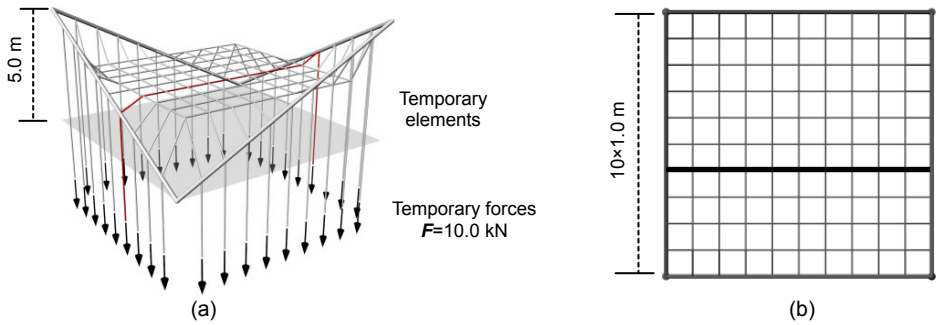

Fig. 11 Initial configuration of the tension structure: (a) side view; (b) top view

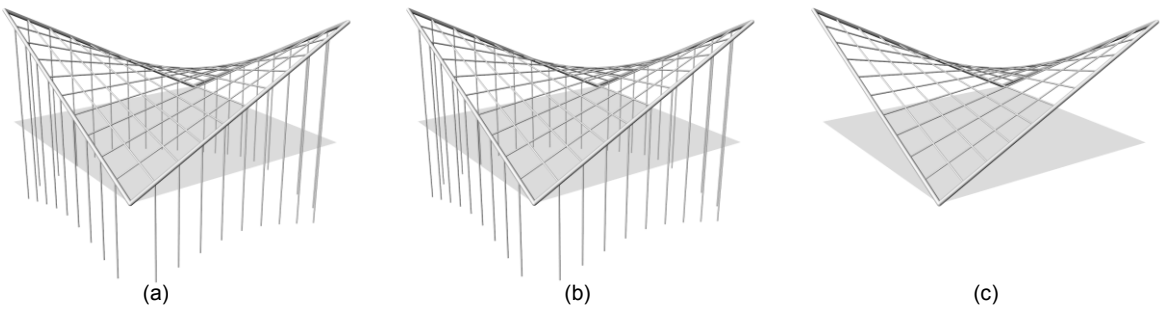

Fig. 12 Comparison of optimized shapes for the tension structure: (a) MDR method; (b) elements-grouped method; (c) generated cable-net structure

when the morphogenesis is completed, so we delete them and obtain the structure shown in Fig. 12c.

The next example, whose initial model is shown in Fig. 13, illustrates how to deal with the problem of free edges. Outside the edges there are 180 temporary elements. In this model, each element in the edges is set as one element group. Each element inside the edges corresponds to a temporary element and they are set as one element group, for instance, the two bold elements shown in Fig. 13a compose one element group. The values of the temporary forces depend on the final structure shape and force-bearing state that the designer expects. The four corner nodes and the top nodes of temporary elements are fixed. The lower nodes of the temporary elements are acted on by vertical downwards nodal loads whose value is 10.0 kN and the other free nodes of the mechanism system are acted on by vertical downwards nodal loads whose value is 1.0 kN.

Fig. 14 shows the evolution of a structural shape. The shape of the edge is changed from polyline to curve during the morphogenesis process. Because the temporary elements are separated out, they do not interfere with the shape of the free edges. Each edge element is set as one element group so the element length is constrained and remains almost constant during the morphogenesis process. We take the ten elements on one edge shown in Fig. 14c to validate the length constraint. The initial lengths and final lengths of these elements are shown in Table 2. The maximum change ratio of element length is about 0.0027%. The length constraint is valid.

In the finite element analysis, the outer diameter of the element modelled as a beam is 5.0 cm and the wall-thickness is 1.0 cm. The nodes in the four corners are fixed. Each node in the structure is acted on by a vertical downwards load (1.0 kN). Figs. 15 and 16 show the moment and axial force distributions for the initial structure and the optimized structure, respectively. In the initial structure, the average bending moment and maximum bending moment are 1.58 kN·m and 3.94 kN·m, respectively. In the optimized structure, the average bending moment and maximum bending moment are 0.47 kN·m and 1.70 kN·m, respectively.

Table 2 Comparison of element lengths

Element number	Initial length, l_0 (m)	Final length, l_n (m)	Change ratio (%)
1	1.1324310	1.1324264	0.0004060
2	1.1324310	1.1324328	0.0001590
3	1.1324310	1.1324382	0.0006358
4	1.1324310	1.1324259	0.0004503
5	1.1324310	1.1324612	0.0026668
6	1.1324310	1.1324575	0.0023400
7	1.1324310	1.1324310	0.0000000
8	1.1324310	1.1324331	0.0001854
9	1.1324310	1.1324340	0.0002649
10	1.1324310	1.1324302	0.0000706

Through the examples, the characteristics of the elements-grouped method are summarized as follows:

1. The method can generate structures featuring predominantly axial force and small bending moment under the given load and this is also the common objective of many structural optimization and form finding methods. However, the resultant shapes generated by different methods are different even if the initial structural shapes are the same because the implementation strategy and features are different.

2. Different settings of element groups lead to a variety of resultant structural shapes, even if the initial model is exactly the same. Hence, the method contributes a new route to structural morphogenesis.

3. If a single element is set as one element group, the method can meet the specific geometry requirement of member length.

4. If more than one element is set as one element group, each element length can change under the condition that the total length is constrained, in other words, each element in this group can self-adjust its length to make the system potential energy decrease. This length self-adjustment function of the method enriches the techniques for generating structural shapes.

5. Through the rational setting of the element group using temporary elements and temporary forces, the method can, to some extent, control the axial forces in the members of the final structure. In fact, the force control is to apply prestress on the linkage mechanism system.

Compared with the DR method, the proposed method focuses on the relationship between geometry and the load under the length constraint and it cannot take into account the material properties. As well known, the functions including the single element length constraint, the axial force control, and the

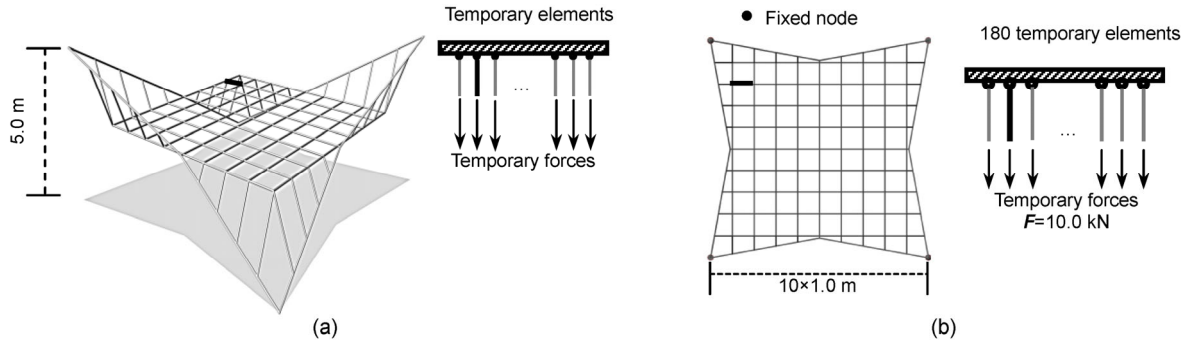

Fig. 13 Initial configuration of the free-edged structure: (a) side view; (b) top view

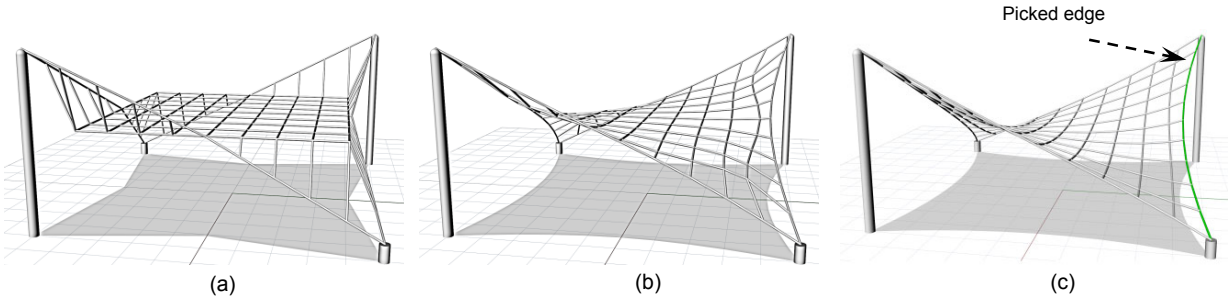

Fig. 14 Evolution of structural shape of free-edged model: (a) step 0; (b) step 500; (c) step 822

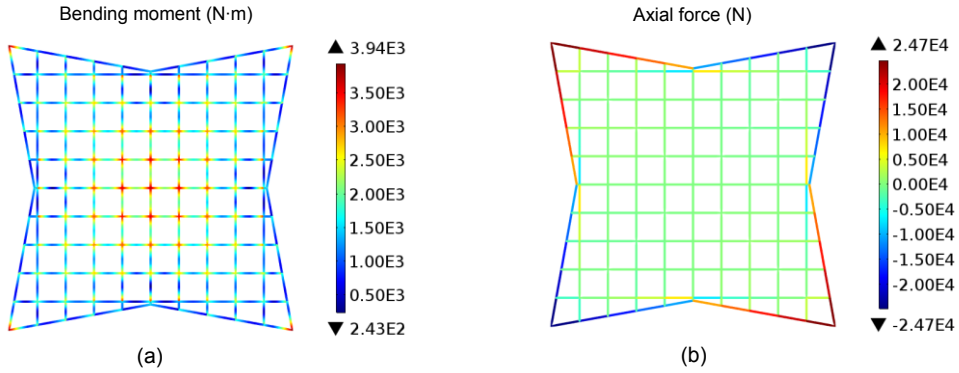

Fig. 15 Bending moment distribution (a) and axial force distribution (b) for the initial free-edged structure

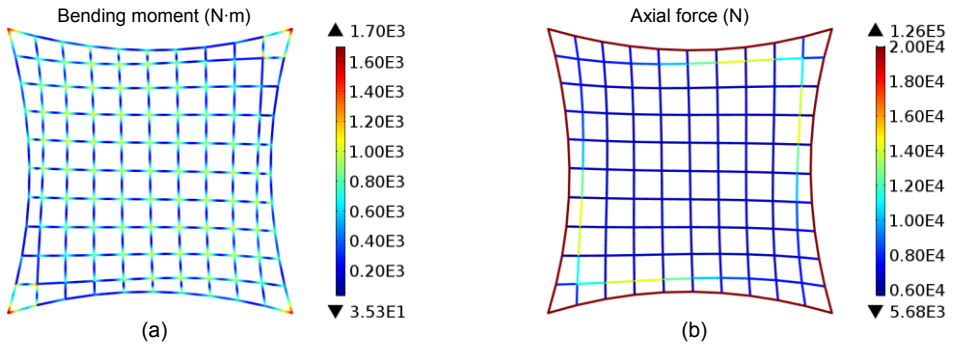

Fig. 16 Bending moment distribution (a) and axial force distribution (b) for the optimized free-edged structure

improvement of mechanical properties can also be implemented by existing form finding methods. However, the elements-grouped method embodies the peculiar functions in the total length constraint and the length self-adjustment.

The total length control leads to many possible shapes as shown in Figs. 4e and 4f because of the redistribution of element lengths in the element group. In addition, geometric factors have a direct impact on the function and shape of the building, so the geometric constraint (single element length constraint and total element length constraint) is very important in the process of structural morphogenesis. The elements-grouped method can directly constrain the member lengths and function in axial force control and length self-adjustment. The integrated use of the functions can generate a variety of rational architectural forms.

4 Design of large-scale structures

In this section, two large-scale design examples are solved in order to prove the validity of the elements-grouped method further. In the finite element analysis, the elastic modulus is 200 GPa, Poisson's ratio is 0.3, and all the members in the structure are treated as beam elements. We assume that the material is linear elastic.

In Fig. 17, six consecutive radial elements with each temporary element are set as an element group marked in bold. For the other elements, each one is set as an element group. Figs. 18a and 18d show the initial configuration selected for the first example. This model consists of five identical parts, one of which is used to illustrate the element group setting. The force acting on each temporary element is 2.0 kN. The other free nodes are acted on by a vertical upwards nodal force whose value is 1.0 kN. In the iterative calculation, the step size is set as Δt=0.001. From the top views in Figs. 18a–18c, the radial element lengths become shorter because the lengths are transferred to temporary elements under the action of

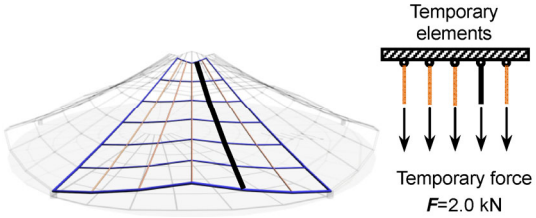

Fig. 17 Setting of element groups

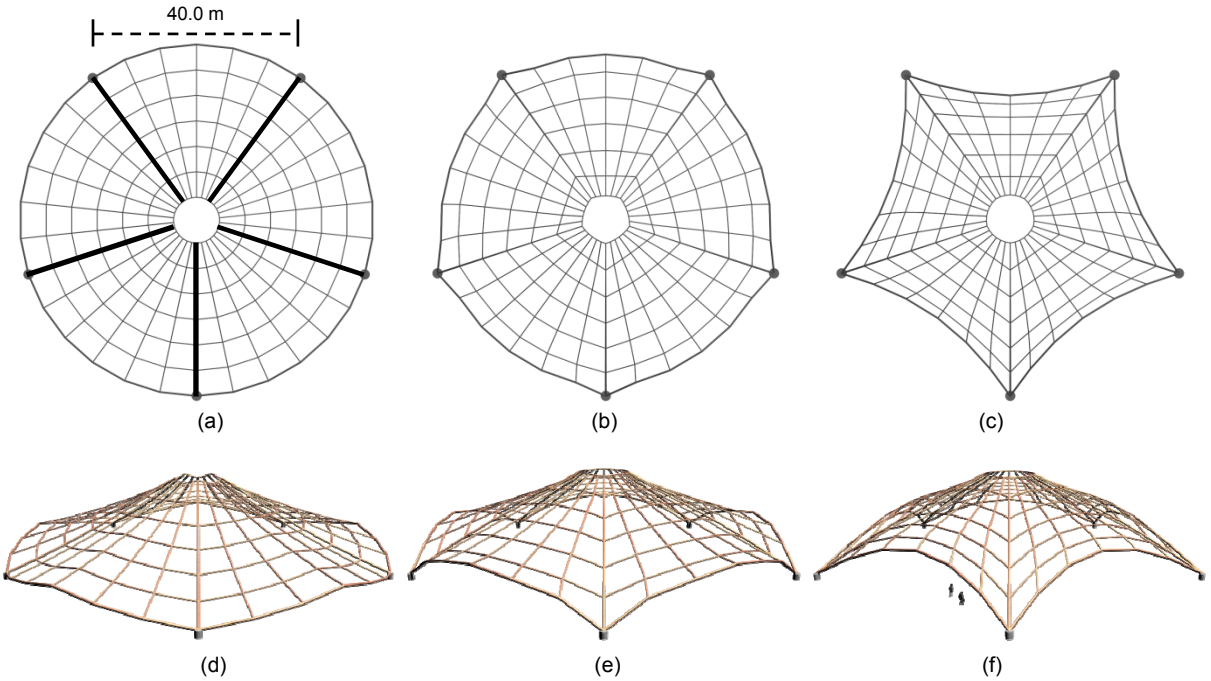

Fig. 18 Morphogenesis process performed for the first large-scale structure considered in this study
Top view of step 0 (a), step 100 (b), and step 1000 (c); Side view of step 0 (d), step 100 (e), and step 1000 (f)

temporary forces. From the side views in Figs. 18d–18f, the free nodes move upwards and the edges assume a parabola-like shape. In view of the overall structure, the structural shape arches up. In this example, the temporary elements and forces make the structural shape look taut. If the temporary elements and forces were not used, the resultant structural shape would look messy and slack although it is rational in mechanical properties. Sometimes setting the temporary elements and temporary forces is also important in controlling the final structural shape. Fig. 19 shows that the potential energy increment of the linkage mechanism system decreases and converges to zero.

In the finite element analysis, the type of the members marked in bold in Fig. 18a is a steel pipe with outer diameter of 25.0 cm and wall thickness of 2.5 cm, and the other members are pipes with outer diameter of 15.0 cm and wall thickness of 1.5 cm. The nodes are acted on by the vertical downwards nodal forces (5.0 kN). Figs. 20a and 20b, respectively, show the distributions of bending moments and axial forces

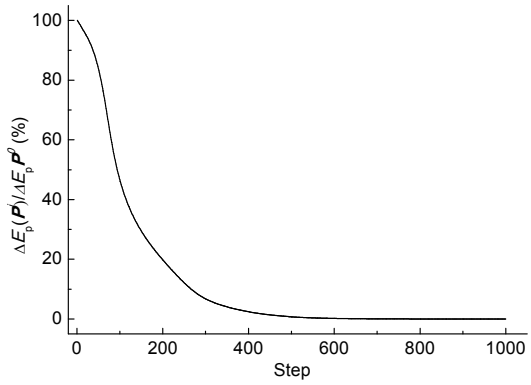

Fig. 19 Variation of potential energy increment in the design process of the first large-scale structure

in the initial structure. For the initial structure, the results of the finite element analysis are as follows:

1. The average bending moment is 12.99 kN·m and the maximum bending moment is 234.04 kN·m.

2. The average axial force is 55.78 kN and the maximum axial force is 387.21 kN.

3. The average nodal displacement is 10.93 cm and the maximum nodal displacement is 22.05 cm.

4. The maximum von Mises stress is 454.75 MPa.

Figs. 21a and 21b, respectively, show the distributions of bending moments and axial forces in the optimized structure. For the optimized structure, the results of the finite element analysis are as follows:

1. The average bending moment is 0.17 kN·m and the maximum bending moment is 1.13 kN·m.

2. The average axial force is 40.65 kN and the maximum axial force is 285.21 kN.

3. The average nodal displacement is 0.28 cm and the maximum nodal displacement is 0.46 cm.

4. The maximum von Mises stress is 16.87 MPa.

Compared with the initial structure, the maximum and average bending moments of the optimized structure decrease by 99.52% and 98.69%; the maximum nodal displacement and the strain energy decrease by 97.91% and 97.44%, respectively; the maximum von Mises stress decreases by 96.29%. The stiffness of the structure is improved. The obtained structure features predominant axial forces and small bending moments under the given loading case. For the elements controlled by the temporary elements, the maximum axial force is 10.83 kN and the minimum axial force is 9.35 kN, whose ideal value is 10.0 kN. Fig. 22 shows an architectural rendering of the resultant structure.

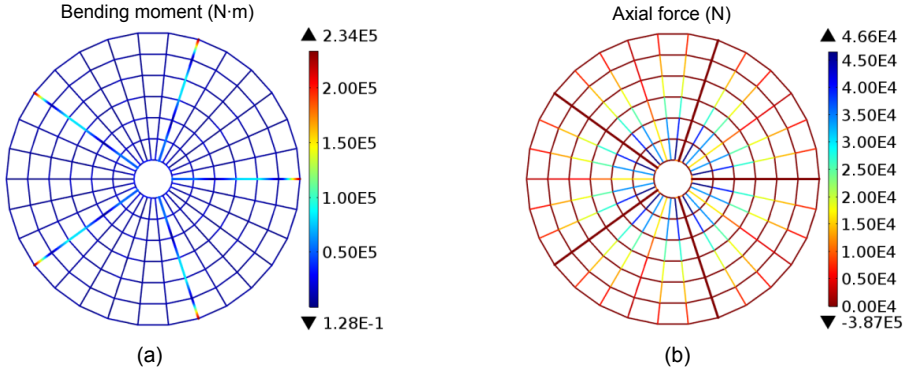

Fig. 20 Distributions of bending moment (a) and axial force (b) for the first large-scale initial structure

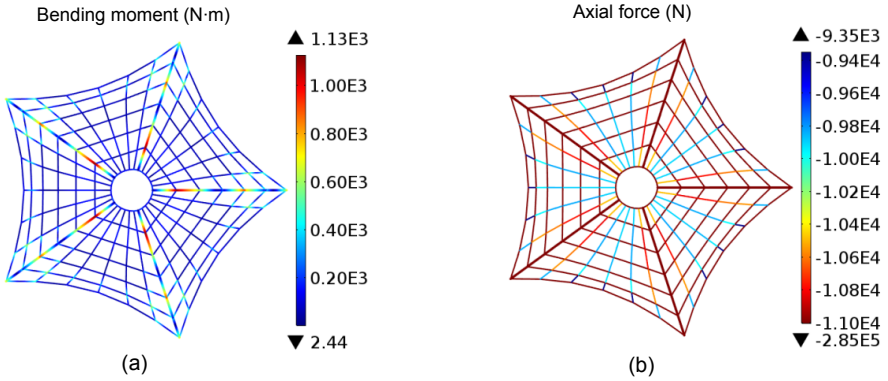

Fig. 21 Distributions of bending moment (a) and axial force (b) for the first large-scale structure designed in this study

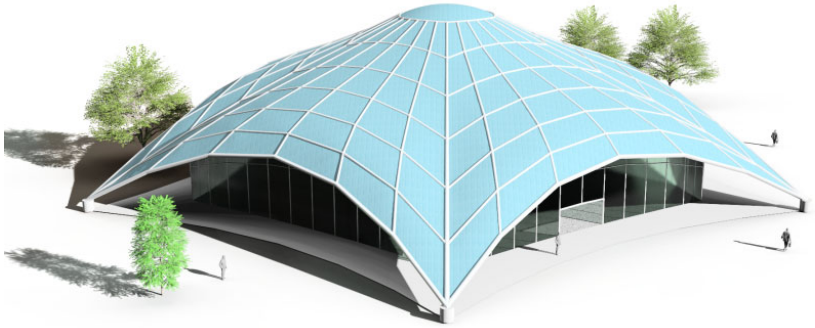

Fig. 22 Architectural rendering for the first large-scale structure designed in this study

We apply the DR method to the initial model shown in Fig. 18d (step 0). Each node is subject to a vertical upward force (1.0 kN). In the computation, each particle mass is 30 kg and the axial stiffness is 600 kN. Fig. 23a shows the structure generated by the DR method. Interestingly, both DR and MDR methods obtained the same result. Compared with the initial structure, the maximum and average bending moments of the optimized structure shown in Fig. 23a decrease by 99.60% and 98.99%, respectively; the maximum nodal displacement decreases by 97.78%; the maximum von Mises stress decreases by 95.83%. Fig. 23b shows the structure in Fig. 18f from another observation position. The comparison above shows that the reduction degrees of the bending moments, maximum nodal displacements, and maximum von Mises stresses of the two structures generated by the two methods are close while the structural shapes are different. The proposed method is characterized by the constraint of the element group length and the settings of the element groups, temporary elements, and temporary forces which can be used to adjust the structural shape.

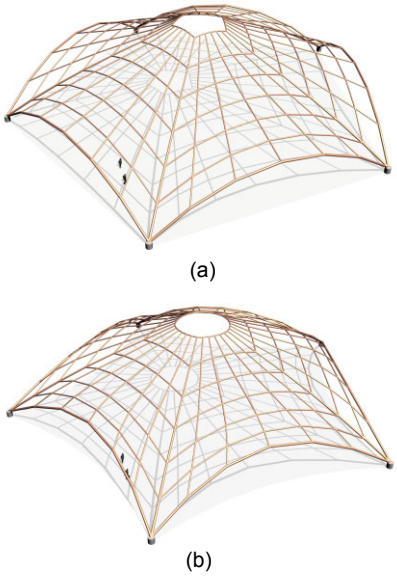

Fig. 23 Structural shapes generated by the DR method (a) and the elements-grouped method (b)

The second large-scale problem solved in this study demonstrates that the elements-grouped method can produce different results for the same initial

model by a comprehensive application of its functions. In this example, we would like to generate a freeform surface grid shell which looks like undulating peaks. Hence, the initial configuration is shown in Fig. 24. The initial model is divided into three domains as shown in Fig. 24a. The six nodes at the bottom are fixed and the other nodes are acted on by vertical upwards nodal forces whose value is 1.0 kN.

Each element in the edge lines in Fig. 24 is set as one element group. For the other elements, we group them using three modes as shown in Fig. 25:

① Each element is set as one element group.

② The elements parallel to each other in a row or column are set as one element group.

③ The elements in a line and a temporary element are set as one element group, for instance, the elements and a temporary element marked in bold in Fig. 25c compose an element group. Each temporary element is acted on by a temporary force. It is worth noting that the temporary force values are determined through trial computation in consideration of the generated structural shape.

Figs. 26–28 show the element grouping schemes based on the three options illustrated in Fig. 25 and the corresponding resultant shapes. The resultant shape in Fig. 26c has three spires of the same height because each element length is constrained. Two spires become domes in Fig. 27c because of the change of element group setting. In Fig. 28c, the height of the domain with the temporary forces becomes lower, and then three different peak shapes appear. From this example, it can be seen that the elements-grouped method can easily provide multiple shapes for architectural design.

As shown in Fig. 29, the convergence speed of option (I) is faster and that is because each element length of the initial model is constrained. The shape change for option (I) is relatively small. From the authors' aesthetic, the structural shape in Fig. 28c is better than the other two.

In the finite element analysis, the type of the members marked in bold in Fig. 28a is the steel pipe with outer diameter of 25 cm and wall thickness of 2.5 cm, and the other members are pipes with outer diameter of 15 cm and wall thickness of 1.5 cm. The nodes are acted on by the vertical downwards nodal forces (5.0 kN). Figs. 30a and 30b (p.860) show respectively the distributions of bending moments and axial forces in the initial structure. For the initial structure, the results of the finite element analysis are:

1. The average bending moment is 188.98 kN·m and the maximum bending moment is 431.18 kN·m.

Fig. 24 Initial configuration selected for the second large-scale design example: (a) top view; (b) side view

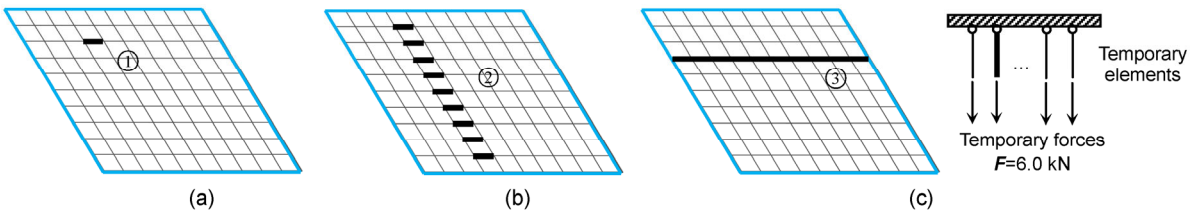

Fig. 25 Element grouping options for the second large-scale design example: (a) the first element grouping mode; (b) the second element grouping mode; (c) the third element grouping mode

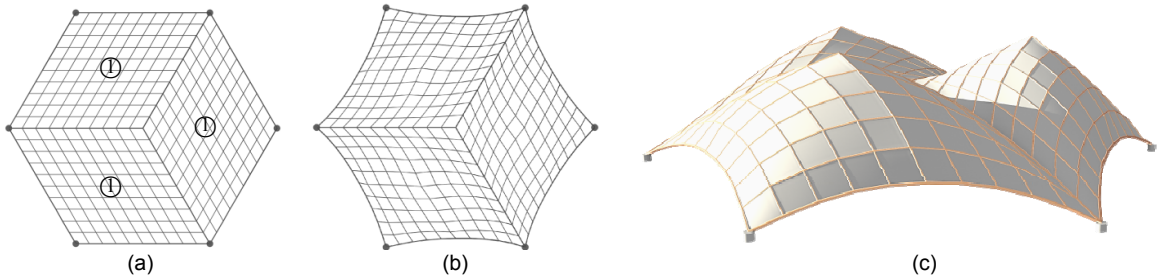

Fig. 26 Design obtained for grouping option (I) in the second large-scale example: (a) element group setting; (b) top view; (c) side view

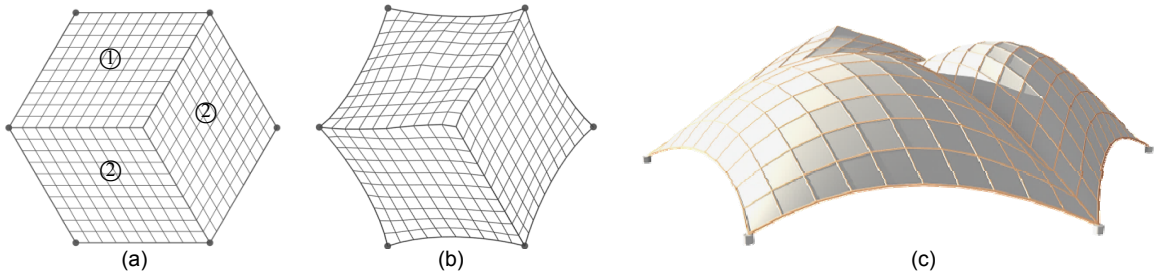

Fig. 27 Design obtained for grouping option (II) in the second large-scale example: (a) element group setting; (b) top view; (c) side view

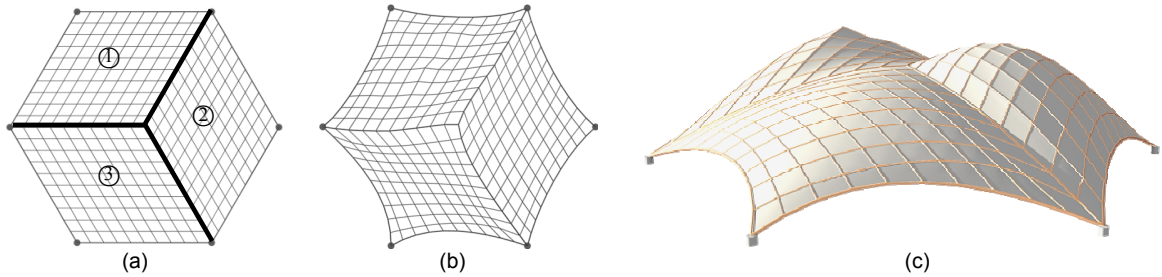

Fig. 28 Design obtained for grouping option (III) in the second large-scale example: (a) element group setting; (b) top view; (c) side view

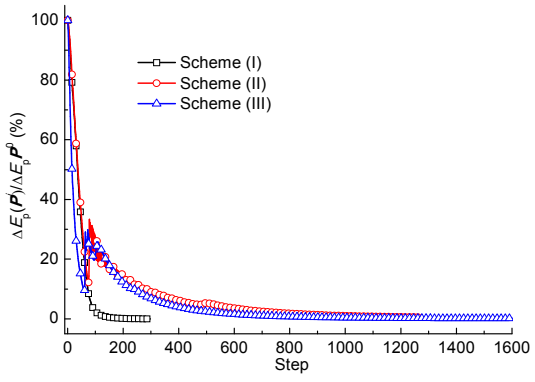

Fig. 29 Variation of potential energy in the design process of the second large-scale structure considered in this study

2. The average axial force is 48.74 kN and the maximum axial force is 625.38 kN.

3. The average nodal displacement is 26.53 cm and the maximum nodal displacement is 45.82 cm.

4. The maximum von Mises stress is 516.42 MPa.

Figs. 31a and 31b show respectively the distributions of the axial forces and the bending moments in the optimized structure. For the optimized structure, the results of the finite element analysis are as follows:

1. The average bending moment is 0.56 kN·m and the maximum bending moment is 8.33 kN·m.

2. The average axial force is 51.95 kN and the maximum axial force is 411.23 kN.

3. The average nodal displacement is 0.82 cm and the maximum nodal displacement is 2.41 cm.

4. The maximum von Mises stress is 75.59 MPa.

The maximum bending moment decreases by 98.07% and the average bending moment decreases by 99.70%; the maximum nodal displacement and the strain energy decrease by 94.74% and 96.91%,

respectively; the maximum von Mises stress decreases by 85.36%. The stiffness of the structure is improved significantly. Fig. 32 shows an architectural rendering of the resultant structure in Fig. 28c.

The DR method and MDR method are used on the initial model shown in Fig. 24. In the computations, each particle mass is 30 kg and the axial stiffness is 600 kN. Each node is subject to a vertical upward force (1.0 kN). Fig. 33a shows the structural shape generated by the DR method. The MDR method can simulate behavior of continuous cables and adjust structural shape through adjusting the setting of continuous cables. Fig. 33b shows the shape generated by the MDR method and the bold elements are continuous cables. Compared with the shapes generated by the DR and MDR methods, the shape

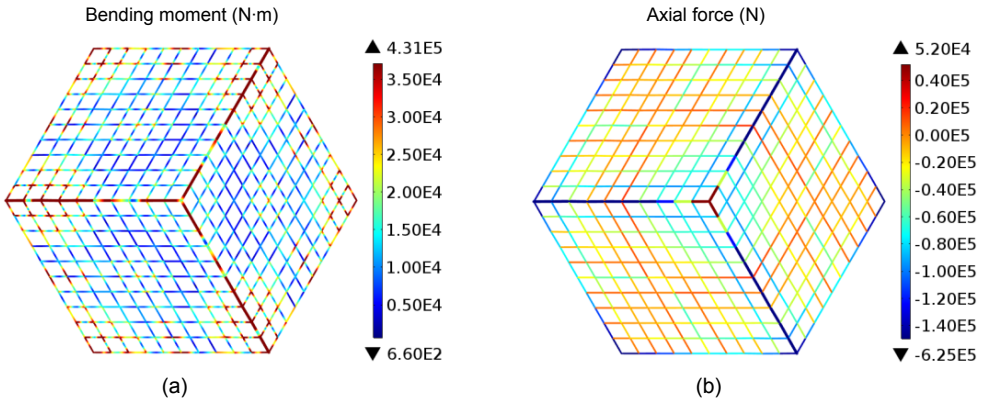

Fig. 30 Distributions of bending moment (a) and axial force (b) for the second large-scale initial structure

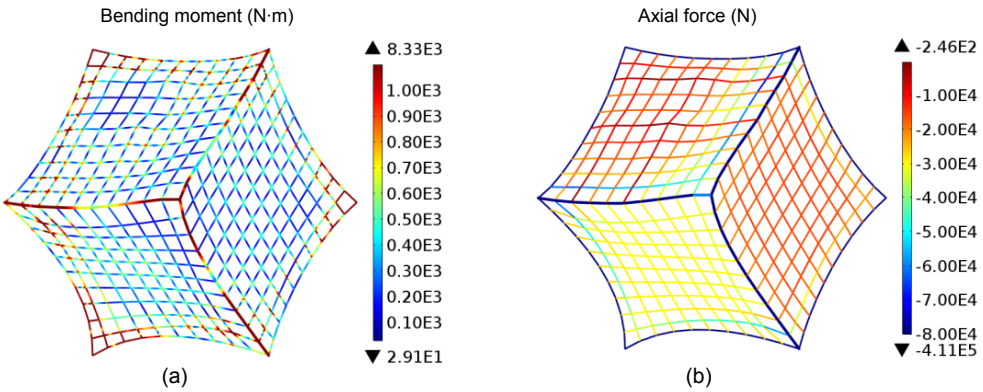

Fig. 31 Distributions of bending moment (a) and axial force (b) for the second large-scale optimized structure

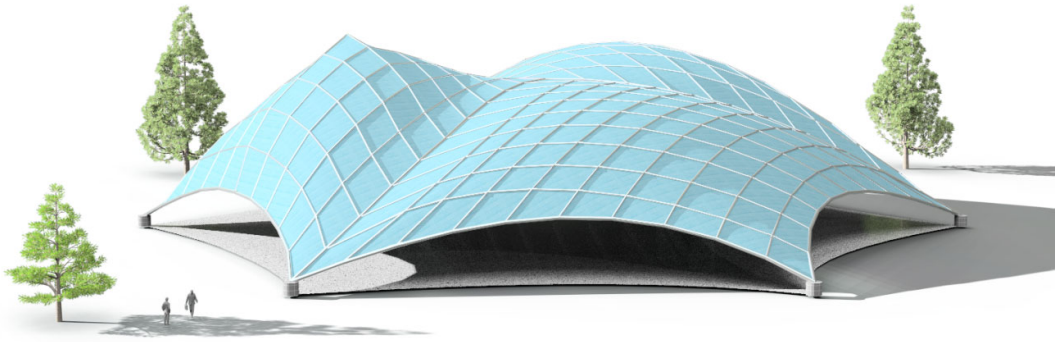

Fig. 32 Architectural rendering for the second large-scale structure designed in this study

(Fig. 26c) generated by the proposed method is slightly different when each element is set as one element group as shown in Fig. 26. However, when the element group settings are changed, the proposed method generates structural shapes that are significantly different from those in Fig. 33, as shown in Figs. 27c and 28c. In addition, the structures generated by the three methods mainly rely on axial forces to resist the given load. However, the proposed method introduces the element grouping manners and the constraint of element group length, which can provide multiple structural shapes through changing the settings of element groups, temporary elements, and temporary forces, and thus it is valuable for architectural shape design.

The proposed method can guarantee that the generated structure carries the given load with smaller bending moments. Thus, it can provide rational structural shape schemes for architectural design. When the structure shape is determined, other tasks including member section design must be carried out to make the structure satisfy requirements for strength, stiffness, and stability.

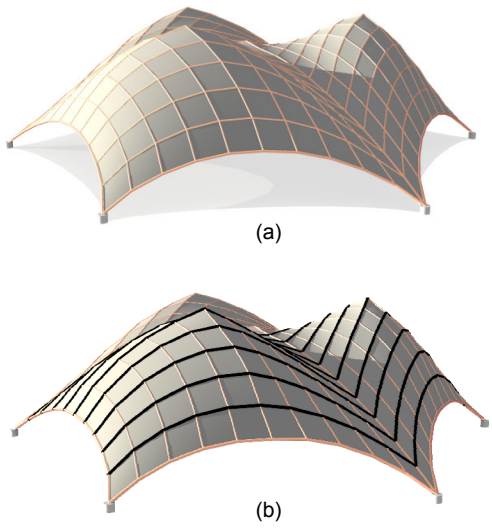

Fig. 33 Structural shapes generated by the DR method (a) and the MDR method (b)

5 Conclusions

This study presented a morphogenesis method, called the elements-grouped method, for designing grid shell structures. The method searches for the shape of the linkage mechanism system corresponding to the minimum potential energy and the structure with the resultant shape features predominantly axial forces under the given load. The length constraint function allows it to satisfy specific geometry requirements of architecture. Different element group settings can lead to various different rational structural shapes for the same initial model, which can offer choices to architects at the schematic design stage. Moreover, the introduction of temporary elements and temporary forces provides an axial force control function and extends the applicability of the method. In total, the functions of the proposed method in length constraint, axial force control, and length self-adjustment enrich the means to generate a large number of structural shapes, and offer more architectural schemes for designers. The design examples given show the efficiency of the proposed method.

References

Adriaenssens S, Block P, Veenendaal D, et al., 2014. Shell Structures for Architecture: Form Finding and Optimization. Routledge, New York, USA.

Adriaenssens SML, Barnes MR, 2001. Tensegrity spline beam and grid shell structures. *Engineering Structures*, 23(1): 29-36. https://doi.org/10.1016/S0141-0296(00)00019-5

Alic V, Persson K, 2016. Form finding with dynamic relaxation and isogeometric membrane elements. *Computer Methods in Applied Mechanics and Engineering*, 300: 734-747. https://doi.org/10.1016/j.cma.2015.12.009

Argyris JH, Angelopoulos T, Bichat B, 1974. A general method for the shape finding of lightweight tension structures. *Computer Methods in Applied Mechanics and Engineering*, 3(1):135-149. https://doi.org/10.1016/0045-7825(74)90046-2

Bagrianski S, Halpern AB, 2014. Form-finding of compressive structures using prescriptive dynamic relaxation. *Computers & Structures*, 132:65-74. https://doi.org/10.1016/j.compstruc.2013.10.018

Barnes MR, 1977. Form Finding and Analysis of Tension Space Structures by Dynamic Relaxation. PhD Thesis, City University London, London, UK.

Barnes MR, 1988. Form-finding and analysis of prestressed nets and membranes. *Computers & Structures*, 30(3): 685-695. https://doi.org/10.1016/0045-7949(88)90304-5

Barnes MR, 1999. Form finding and analysis of tension structures by dynamic relaxation. *International Journal of Space Structures*, 14(2):89-104. https://doi.org/10.1260/0266351991494722

Barnes MR, Adriaenssens S, Krupka M, 2013. A novel torsion/bending element for dynamic relaxation modeling. *Computers & Structures*, 119:60-67. https://doi.org/10.1016/j.compstruc.2012.12.027

Bel Hadj Ali N, Rhode-Barbarigos L, Pascual Albi AA, et al., 2010. Design optimization and dynamic analysis of a tensegrity-based footbridge. *Engineering Structures*, 32(11):3650-3659. https://doi.org/10.1016/j.engstruct.2010.08.009

Bel Hadj Ali N, Rhode-Barbarigos L, Smith IFC, 2011. Analysis of clustered tensegrity structures using a modified dynamic relaxation algorithm. *International Journal of Solids and Structures*, 48(5):637-647. https://doi.org/10.1016/j.ijsolstr.2010.10.029

Bletzinger KU, Ramm E, 1999. A general finite element approach to the form finding of tensile structures by the updated reference strategy. *International Journal of Space Structures*, 14(2):131-145. https://doi.org/10.1260/0266351991494759

Bletzinger KU, Wüchner R, Daoud F, et al., 2005. Computational methods for form finding and optimization of shells and membranes. *Computer Methods in Applied Mechanics and Engineering*, 194(30-33):3438-3452. https://doi.org/10.1016/j.cma.2004.12.026

Block P, Ochsendorf J, 2007. Thrust network analysis: a new methodology for three-dimensional equilibrium. *Journal of the International Association for Shell and Spatial Structures*, 48(3):167-173.

Cui CY, Jiang BS, Wang YB, 2014. Node shift method for stiffness-based optimization of single-layer reticulated shells. *Journal of Zhejiang University-SCIENCE A* (*Applied Physics & Engineering*), 15(2):97-107. https://doi.org/10.1631/jzus.A1300239

Day AS, 1965. An introduction to dynamic relaxation. *The Engineer*, 219(5688):218-221.

Descamps B, Filomeno Coelho R, Ney L, et al., 2011. Multicriteria optimization of lightweight bridge structures with a constrained force density method. *Computers & Structures*, 89(3-4):277-284. https://doi.org/10.1016/j.compstruc.2010.11.010

Gosling PD, Lewis WJ, 1996. Optimal structural membranes —II. Form-finding of prestressed membranes using a curved quadrilateral finite element for surface definition. *Computers & Structures*, 61(5):885-895. https://doi.org/10.1016/0045-7949(96)00091-0

Haber RB, Abel JF, 1982. Initial equilibrium solution methods for cable reinforced membranes part I—formulations. *Computer Methods in Applied Mechanics and Engineering*, 30(3):263-284. https://doi.org/10.1016/0045-7825(82)90080-9

Hangai Y, Kawaguchi KI, 1987. Shape-finding analysis of unstable link structures. *Journal of Structural and Construction Engineering*, 381:56-60. https://doi.org/10.3130/aijsx.381.0_56

Haug E, Powell GH, 1972. Analytical shape finding for cable nets. Proceedings of the IASS Pacific Symposium Part II on Tension Structures and Space Frames, p.83-92.

Isler H, 1994. Concrete shells derived from experimental shapes. *Structural Engineering International*, 4(3):142-147. https://doi.org/10.2749/101686694780601935

Jorquera Lucerga JJ, Armisen JM, 2012. An iterative form-finding method for antifunicular shapes in spatial arch bridges. *Computers & Structures*, 108-109:42-60. https://doi.org/10.1016/j.compstruc.2012.02.015

Kilian A, Ochsendorf J, 2005. Particle-spring systems for structural form finding. *Journal of the International Association for Shell and Spatial Structures*, 46(2):77-84.

Maurin B, Motro R, 1998. The surface stress density method as a form-finding tool for tensile membranes. *Engineering Structures*, 20(8):712-719. https://doi.org/10.1016/S0141-0296(97)00108-9

Maurin B, Motro R, 2004. Concrete shells form-finding with surface stress density method. *Journal of Structural Engineering*, 130(6):961-968. https://doi.org/10.1061/(asce)0733-9445(2004)130:6(961)

Moored KW, Bart-Smith H, 2009. Investigation of clustered actuation in tensegrity structures. *International Journal of Solids and Structures*, 46(17):3272-3281. https://doi.org/10.1016/j.ijsolstr.2009.04.026

Pauletti RMO, Pimenta PM, 2008. The natural force density method for the shape finding of taut structures. *Computer Methods in Applied Mechanics and Engineering*, 197(49-50):4419-4428. https://doi.org/10.1016/j.cma.2008.05.017

Sánchez J, Serna MÁ, Morer P, 2007. A multi-step force-density method and surface-fitting approach for the preliminary shape design of tensile structures. *Engineering Structures*, 29(8):1966-1976. https://doi.org/10.1016/j.engstruct.2006.10.015

Schek HJ, 1974. The force density method for form finding and computation of general networks. *Computer Methods in Applied Mechanics and Engineering*, 3(1):115-134. https://doi.org/10.1016/0045-7825(74)90045-0

Shan J, Lan T, 1994. On dynamic relaxation and its application to static analysis of tension structures. *Journal of Southeast University*, 24(3):94-98 (in Chinese).

Siev A, Eidelman J, 1964. Stress analysis of prestressed suspended roofs. *Journal of the Structural Division*, 90(4): 103-121.

Xie YM, Steven GP, 1993. A simple evolutionary procedure for structural optimization. *Computers & Structures*, 49(5):885-896. https://doi.org/10.1016/0045-7949(93)90035-C

Zhang L, Lu MK, Zhang HW, et al., 2015. Geometrically nonlinear elasto-plastic analysis of clustered tensegrity based on the co-rotational approach. *International Journal of Mechanical Sciences*, 93:154-165. https://doi.org/10.1016/j.ijmecsci.2015.01.015

中文概要

题　目： 基于联动机构的结构形态创构方法

目　的： 寻找以轴力为主要传递荷载方式的单层网壳结构的多种合理形态，改善结构的受力性能，为建筑设计提供多种合理的结构形状方案。

创新点： 1. 建立控制单元组长度的移形方程，并在移形方程的基础上推导基于联动机构势能最小化的结构形态创构方法。2. 将分组方式应用于网壳结构形态创构，并通过改变分组形式获得不同的合理结构形状；临时单元与临时力的引入拓展了方法的适用范围，也为形态创构提供了新的途径。

方　法： 1. 将机构的单元进行分组，以单元组总长度不变作为条件建立机构移形方程；根据机构势能下降最快的方向调整机构形状，使机构逐步达到势能最低。2. 在同一初始模型中，通过改变临时单元、临时力以及单元组的设置来获得多种合理结构形状；通过多个数值算例说明该方法的特性。3. 对该方法所生成的结构进行受力性能分析，验证所提方法的可行性和有效性。

结　论： 提出了一种适用于网壳结构的形态创构方法。该方法简单、灵活，可以通过调整临时单元、临时力以及单元组的设置，得出多种以轴力为主要传递荷载方式的合理结构形状。可以为设计者在建筑方案设计阶段提供多种结构形状方案。

关键词： 形态创构；单元分组；联动机构；长度约束；长度自调整